Chapter 2
The Molecular Universe

Maryvonne Gerin

Abstract This chapter presents a description of the interstellar medium. It starts with a summary of the interstellar medium structure and how the various phases are related to each other. The emphasis is put on molecular clouds, and on their densest regions, the dense cores, which are the birth place of stars. The evolution of matter during the star formation process and its observable consequences, especially in term of chemical composition is presented. The next section is dedicated to the constituents of the interstellar medium, with separate presentations of the gas species and the dust grains. Methods used by astronomers to derive useful information on the structure, temperature, ionization rate of interstellar environments as well as magnetic fields are briefly described. The last part of the chapter presents the telescopes and their instruments used for studying the interstellar medium across the electromagnetic spectrum.

2.1 Introduction

The formation of the first galaxies is now understood in the large scale context of the evolution of the Universe. Starting from the first seeds evidenced as tiny fluctuations in the Cosmic Microwave Background (CMB), the combined actions of expansion and gravity led to the growth of large scale structures, in the form of sheets and filaments of denser material, surrounded by large voids. Baryons condensed in the filaments to form the first stars and galaxy embryos. The first stages of this evolution were dominated by dark matter since the dark matter haloes were far larger in size and mass than individual galaxies, and therefore dominated the gravitational potential. Conversely, the last steps in the formation of galaxies and stars within these dark matter haloes were governed by the non-linear physics

M. Gerin (✉)
LERMA (Observatoire de Paris, CNRS and ENS), Paris Cedex 05 FR 75321, France
e-mail: maryvonne.gerin@lra.ens.fr

I.W.M. Smith et al. (eds.), *Astrochemistry and Astrobiology*, Physical Chemistry in Action,
DOI 10.1007/978-3-642-31730-9_2,

of the visible matter. This includes the complex cooling and heating effects of neutral and molecular gas, the action of magnetic fields on the large scale flows of matter, as well as the important dynamical and radiative feedback effects created by newly formed stars. Indeed as soon as a first generation of stars had been formed, the so-called Population III stars, the interstellar medium became enriched in heavy elements (compared to the initial composition resulting from the primordial nucleosynthesis shortly after the Big Bang), leading to more possibilities for cooling and heating the gas, and an easier synthesis of molecules.

The presence of molecules in high redshift massive galaxies [1] as well as in some absorption systems [2] is remarkable given the young age of the Universe at such redshifts: for instance $z = 6$ corresponds to less than 10^9 years after the Big Bang while the age of the Sun and the Solar System is 4.6×10^9 years. It demonstrates the very strong similarities of processes occurring along the whole evolutionary path, and the need for a rather fast formation of dust grains and molecules, at least in the most massive and densest systems. Stars contribute to the enrichment of the interstellar medium by ejecting matter outside of their envelope. This stellar matter, composed both of molecular gas and dust grains, contains the elements synthesized in the stellar core that are transported to the stellar surface and envelope by strong convective motions. In astrophysics, the term 'heavy elements' refers to those elements heavier than boron, which are only synthesized in stars. Therefore they include carbon, oxygen, and nitrogen for instance.

2.2 The Life Cycle Interstellar Medium

2.2.1 Phases of the Interstellar Medium

In the Milky Way, the interstellar medium has distinct phases that result from the interplay of radiation, large scale flows, magnetic fields and turbulence in the gas. Those phases are close to pressure equilibrium, with a median pressure[1] of p~3,500 K cm^{-3}, which implies that the hottest phases have the lowest average particle densities. Table 2.1, adapted from Draine [3] presents the properties of the main interstellar phases.

The structure of the interstellar medium phases, and especially how they are spatially organized, is not fully elucidated. Large scale surveys of tracers of the neutral, ionized and coronal gas have led to determination of the global filling factors, and of the average physical conditions as listed in Table 2.1. The coronal gas, with temperatures in excess of 10^5 K is mostly formed by the bubbles created in

[1] It is customary to quote interstellar pressures as the product of the temperature and particle density, since the equation of state of ideal gas applies to these very dilute media (PV = nRT).

Table 2.1 Summary of interstellar phases (Adapted from Draine [3])

Phase	T/K	n/cm^{-3}	Volume (%)	Mass (%)
Coronal gas	$10^{5.5}$–10^{7}	0.004	50	<1
Warm ionized medium	$\sim 10^{4}$	0.3	10	23
Warm neutral medium	~5,000	0.6	40	36
Cold neutral medium	40–100	~30	1	24
Diffuse molecular gas	30–100	30–300	0.1	0.17
Dense molecular cores	6–50	10^{3}–10^{6}	0.01	<0.05
HII regions	10^{4}	10^{2}–10^{4}	0.01	<0.01

supernovae explosions and other energetic events. Because of its extreme temperature, this component represents a small fraction of the mass, but fills a significant fraction of the Galaxy volume. Most of the mass of ionized gas resides in the Warm Ionized Medium (WIM), a widely distributed component of the interstellar gas. This medium is kept ionized by the combined ionizing radiations of the massive stars of stellar types O and B, and to a lesser degree from other stellar populations such as white dwarfs.

Dynamical models (e.g. [4, 5]) have been constructed to study the formation of these phases and their interplay. The whole pattern is dynamical, with supernovae explosions and stellar winds from massive stars creating bubbles of hot gas expanding through the diffuse medium, accompanied by large scale motions and shock waves.

2.3 The Structure of the Neutral Interstellar Gas

While the warm ionized phases occupy most of the volume of the galaxy, they correspond to a relatively small fraction of the total mass. For star formation as well as for understanding molecular complexity, it is natural to focus on the phases where the hydrogen is in neutral form, either atomic or molecular.

Large scale surveys have established the overall spatial distribution and structure of these phases. The neutral atomic gas can exist in two stable phases, called the Warm Neutral Medium (WNM) and the Cold Neutral Medium (CNM) following the pioneering work of Field et al. [6]. These phases are roughly in pressure equilibrium with a median pressure of ~3,500 K cm^{-3} [7]. Observations of the HI hyperfine transition at 21 cm have confirmed the presence of these stable phases [8], but have also revealed that a significant fraction of the gas resides in the thermally unstable region of the pressure/density diagram. As for the ionized phases, it appears that the neutral gas is not in a static equilibrium, and continuously evolves from one phase to the other. Audit and Hennebelle [9] among others have performed extensive simulations of the dynamics of such a bistable medium.

In the cold neutral medium, hydrogen is not uniquely present in atomic form. Indeed, molecular hydrogen, together with other molecules with a small fractional

abundance (of the order of 10^{-8}) are known to be present in the diffuse gas. The fraction of hydrogen in molecular form, $f(H_2) = 2N(H_2)/(N(HI) + 2\,N(H_2))$ varies from less than 10% in low extinction regions ($A_V \leq 0.1$ mag), up to nearly 100% in translucent gas with extinctions of a few magnitudes [10].

The overall structure of the diffuse neutral gas therefore appears to be governed by the interplay of radiation, turbulence and magnetic fields, with its specific equation of state. The structure of this diffuse gas is best studied by the HI 21 cm emission, and by the far infrared and sub-millimetre dust emission between 100 and 900 μm. The typical temperature of dust grains in these regions is 18 K, hence they radiate mostly at far infrared wavelengths. The IRAS satellite, followed by more powerful space missions (ISO, Spitzer, Herschel), have produced sensitive and large scale images of the dust thermal radiation at far infrared wavelengths, leading to a good statistical characterization of the structure. It is remarkable that the structure follows the same statistical properties from spatial scales of 8° down to 30″ (∼15 to ∼0.015 pc, where one parsec (pc) corresponds to 3.08×10^{16} m or about 3.26 light years) in the Polaris diffuse cloud [11]. Large scale flows induced by dynamical events, combined with turbulence, stir the gas and induce local compressions where cold neutral medium cloudlets can form. Numerical simulations have been performed to study the formation and evolution of the atomic gas (e.g. [9]). The simulated structures share many statistical properties with the interstellar gas, demonstrating that the main physical ingredients are well captured by such simulations.

Gravity becomes important in understanding the formation of more massive structures, the molecular clouds. Indeed, giant molecular clouds (GMCs) are the most massive structures in the Galaxy, with masses up to 10^7 $M_\odot$. The giant molecular clouds are located at the upper end of the hierarchical organization of molecular clouds, and follow the same scaling laws, with their mass (M) varying approximately as the square of their radius (R), and their internal velocity dispersion (σ) as the square root of their radius [12]. These scaling laws can be understood as revealing the interplay of the main acting forces, gravity, turbulence and magnetic fields. Indeed, for a system in virial equilibrium it is expected that the gravitational energy (scaling as $G\,M^2/R$) is balanced by the kinetic energy (scaling as $M\sigma^2$), which leads to the near constancy of the factor $M\sigma^2/R$. These scaling laws are reminiscent of the scaling laws for incompressible turbulence, that relate the scale size l and the local velocity dispersion at this scale δv as $l \sim \delta v^\alpha$. The exponent α that depends on the properties of turbulence is expected to be 1/3 for incompressible turbulence as first predicted by Kolmogorov [13]. In the interstellar medium, the scaling deviates from pure incompressible turbulence behaviour, as expected from the more complex nature of the interstellar medium (see [14] for a recent introduction).

2.3.1 Dense Interstellar Cores

2.3.1.1 Low Mass Cores

While the mean density remains moderate in the diffuse interstellar medium and in molecular clouds, with typical figures ranging between 100 and 1,000 cm^{-3}, high density regions, i.e. regions with densities larger than 10^4 cm^{-3} exist, but they occupy a small fraction of the total volume (Table 2.1). Such high density regions are called "dense cores", since they have specific properties compared to the diffuse and medium density medium: in addition to their higher density, they are associated with larger total gas column densities, smaller velocity dispersions, and, before stars form, cooler temperatures than their surrounding medium.

The excellent imaging capabilities of the Herschel space telescope have revealed, with unprecedented detail, the structure of molecular clouds and the regions where dense cores are formed. It is now clear that dense cores form within the ubiquitous filamentary structure of interstellar clouds, as localized density and column density maxima. There is a threshold in gas column density for dense core formation, estimated to be at extinctions of seven magnitudes from the analysis of either deep extinction images [15] or dust sub-millimetre emission maps [16]. With such a threshold, the dense cores will be commonly well shielded from the far ultra violet (FUV) radiation, with some exceptions in massive star forming regions or in photodissociation regions (PDRs) where dense molecular gas becomes directly exposed to FUV radiation.

It is now well established that dense cores are the birthplaces of stars. Most cores have relatively low masses, comparable or slightly larger than the mass of the sun, and will be able to form low mass stars like the sun only. The dense cores localized in the nearby molecular clouds such as the Taurus and Perseus complexes have been identified and catalogued through extensive surveys in the last decades. Dense cores are cold objects, with inner temperatures of about 10 K. Their typical size is 0.1 pc (3.08×10^{15} m, or 20,000 AU), and the typical line widths of molecular lines range between 0.2 and 0.6 km s^{-1}, a figure comparable with the thermal velocity dispersion of molecular hydrogen at a kinetic temperature of 10 K (0.2 km s^{-1}). The dark cloud Barnard 68 illustrated in Fig. 2.1 is considered as a model object of this class. Located at a distance of 125 pc, it appears as a dark patch hiding the stellar background. Although not completely axisymmetric, it can be well described as a spherical object, with a smoothly varying density profile that can be well fitted with a so-called Bonnor-Ebert profile, of the class of self-similar solutions of self gravitating isothermal gas spheres. This class of profiles is characterized by an inner plateau of nearly constant density, and a steep density decrease at the edge, scaling as r^{-2}, r being the local radius. In the case of Barnard 68, the maximum density is $n \sim 2.5 \times 10^5$ cm^{-3}. Barnard 68 does not host any young star or proto-stellar object, and seems to be in quasi-static equilibrium. Other dense cores show more concentrated profiles (e.g. LDN 1544 [18]) indicating that they are on the verge of collapse. Dense cores without sign of star formation are

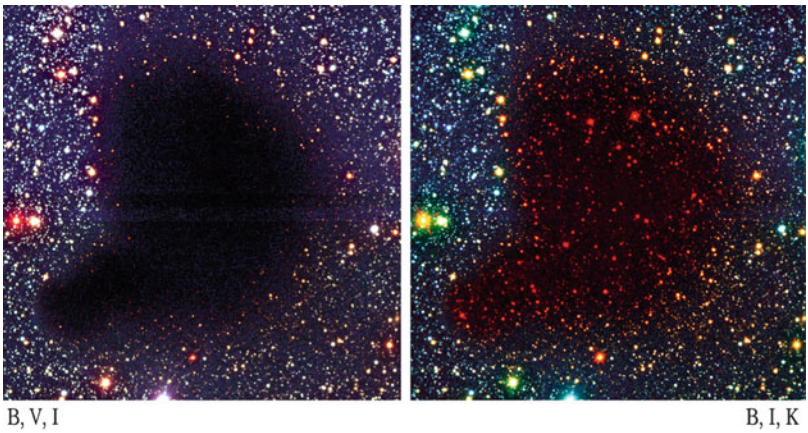

Fig. 2.1 Image of the Barnard 68 dark cloud at visible wavelengths (*left*) and combining with near infrared (J, H and K coded with *red colour*) (*right*). This dense interstellar core blocks the light of the background stars, creating a dark patch. The dust grains responsible for this visible extinction are less effective in the infrared, enabling the detection of the brightest stars (Courtesy ESO, J. Alves [17])

called pre-stellar cores, and represent the initial conditions for the birth of stars, while those already hosting newly formed young stellar objects are called proto-stellar cores. Pre-stellar cores usually are colder and less turbulent than proto-stellar cores.

2.3.1.2 High Mass Cores

Finding the counterparts of the low mass dense cores for high mass stars has proven to be more difficult for several reasons

- The massive star forming regions are statistically more distant than the low mass star forming regions, leading to limited spatial resolution and a more difficult recognition of small compact objects.
- Massive stars are less numerous than low mass stars implying a smaller number of progenitors and the need to survey large areas in the sky to build statistically significant samples.
- Massive stars evolve significantly faster than low mass stars, and have a strong effect on their surrounding environment due to the combined effect of strong winds and radiation. Their birthplace must therefore be identified at a very early stage, before these negative feedback effects have had time to develop.

The best method for finding birth places of massive stars has been to use extensive surveys of large areas of the Galactic plane, either at sub-millimetre wavelengths targeting the dust thermal emission, or at mid infrared wavelengths targeting the PAH emission and the dust extinction. Indeed, the most massive cores

are recognized as compact sub-millimetre sources and/or by maxima of the infrared extinction, two diagnostics of large column densities approaching 100 magnitudes of visual extinction, or H_2 column densities larger than 10^{23} cm^{-2}. The objects detected in the infrared are called "Infrared dark clouds" to mimic the name of the classical "dark clouds" such as Barnard 68. First recognized in the ISO imaging data [19], their study has rapidly developed using the subsequent infrared satellites WISE and Spitzer. As of today, the most recent catalogue contains over 10,000 objects [20]. A careful and lengthy work of cross identification and validation must be performed, after a particular object has been detected, to determine its nature. Although the search for massive pre-stellar cores is a rapidly evolving field, it is already well accepted that a fraction of the IR dark clouds belongs to this category, while other IR dark clouds already harbour massive proto-stars and are therefore at a later stage of evolution. The massive proto-stellar cores are typically located at larger distances than the local pre-stellar cores, because they are associated with larger molecular clouds that are relatively rare in the solar neighbourhood. They have larger masses too, typically of a few tens solar masses, sufficient to enable the formation of at least one massive star. Otherwise, their physical conditions and chemical composition are fairly similar to those of pre-stellar cores, with a tendency towards slightly warmer temperatures.

2.3.2 *Young Stellar Objects and Their Environment*

After the onset of gravitational collapse of a dense core, and when a first stellar embryo is formed, the physical conditions and chemical composition of the surrounding envelope are heavily modified. The increase of temperature due to the infrared radiation produced by the accreting object, combined with shocks and outflows and eventually with energetic radiation (FUV, X-rays) produced by the young proto-stars lead to a strong increase of the temperature in a small zone around the proto-star. This leads to the destruction of ice mantles, either through thermal evaporation or through non-thermal processes like sputtering by shocks or photo-desorption. The presence of relatively complex organic species such as methyl formate ($HCOOCH_3$) or dimethyl ether ($(CH_3)_2O$) as well as a tenfold increase of the abundance of formaldehyde (H_2CO) or methanol (CH_3OH) are clear signs of this phenomenon as explained in the review by Herbst and van Dishoeck [21].

The large number of complex molecules leads to a rich spectrum in the millimetre and sub-millimetre wavelength range, with numerous spectral lines. Two object classes are defined, that depend on the mass of the associated proto-star: high mass sources are called "hot cores", while the term "hot corinos" refers to solar type proto-stars. Indeed, because the time scales for low mass and high mass star formation are different, with high mass stars evolving significantly more rapidly than low mass stars, it is expected that clues on the chemical mechanisms will be found by studying both categories. Among the important differences, one must take into account the longer evolutionary time scale for low mass star

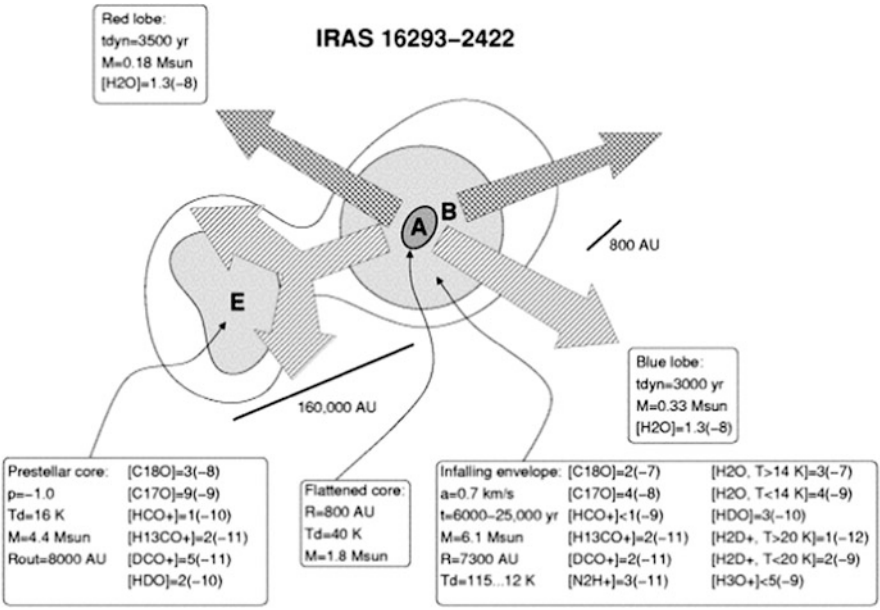

Fig. 2.2 Sketch of the environment of the low mass proto-star IRAS16293-2422 [23]. A binary system with sources A and B is located at the centre of a cold dense core. Sources A and B have distinct chemistries with a richer composition of organic species in source A. This system is associated with two molecular outflows, in the East–west and North-East-South-West directions represented by *arrows*. The former outflow is compressing a second dense core to the East (core E), triggering a new generation of star formation

formation, and the smaller envelope mass that leads to a lesser degree of processing of the species produced in the ice mantles in low mass proto-stars, compared to the hot cores in high mass star forming regions. The degree of deuterium fractionation is significantly larger in hot corinos compared to hot cores with relatively easy detections of doubly deuterated formaldehyde and even triply deuterated methanol in the prototypical source IRAS16293-2422 [22].

A key characteristic of young proto-stars is the presence of bipolar molecular outflows and jets as shown in Figs. 2.2 and 2.6. These collimated structures have a strong impact on the dense core where the proto-star is born, by stirring and disrupting the quiet cocoon. As explained below, the jets and outflows are connected with the accretion of matter on the central object, and contribute to the outward transport of energy and angular momentum that is necessary for energy and angular momentum conservation. These jets and outflows also have interesting chemical properties: because sputtering is efficient in shocks where dust grains are bombarded with atoms and molecules from the gas phase, grain mantles, and even a fraction of the grain cores, are destroyed in the molecular outflows. This leads to a specific chemistry, with significant enrichment of the shocked gas in some molecular species such as silicon monoxide (SiO) and water vapour (H_2O). Molecular outflows show up as broad "wings" in the molecular line profiles, tracing the

presence of material at different velocities (either more positive or red-shifted, more negative or blue-shifted, or both) than the dense core, with a roughly symmetrical pattern of blue-shifted emission on one side of the proto-star and red-shifted emission on the other side (Fig. 2.2). Such a pattern can be analysed to deduce the expansion velocity, the opening angle as well as the orientation of the bipolar outflow on the plane of the sky. While molecular outflows are easily detectable in rotational lines of carbon monoxide (CO), care must be taken to separate the outflow signal from the emission associated with the dense molecular core. Other species are used that provide a better contrast, silicon monoxide or water vapour. The presence of strong emission from silicon monoxide, a species directly linked to the destruction of the silicates cores, as well as from water vapour, the main constituent of grain mantles, are two strong arguments supporting the destruction of mantles in such shocks. Molecular outflows are therefore good places to study the influence of shocks on the structure of the interstellar medium, as well as physical processes, especially the sputtering of ice mantles and grain cores.

The presence of magnetic fields has a strong influence on the process of star formation, because it introduces an asymmetry in the collapse and permits an efficient angular momentum transfer in the first stages of the gravitational collapse. Recent theoretical studies (e.g. [24] and references therein) based on extensive MHD simulations, have shown that the gravitational collapse proceeds with the formation of a flattened structure (a "pseudo-disk") and the launching of outflows. The fragmentation into several components, as well as the formation of a Keplerian disk depends on one key parameter, the mass to flux ratio $\mu = (M_0/\Phi)/(M/\Phi)_c$, relating the core mass M_0, the magnetic flux $\Phi = \pi B R_0^2 = \pi B(3\ M_0/4\pi\rho)^{2/3}$ and the critical value of the mass to magnetic flux ratio $(M/\Phi)_c = (c_1/3\pi)\ \sqrt{(5/G)}$ where c_1 is a numerical constant of about 0.53 [25]. Large values of μ (>20) correspond to a behaviour approaching the pure hydrodynamical case, while small values of μ (<0.1) correspond to a behaviour dominated by the magnetic field. Typical values deduced from the observations correspond to $\mu \sim 2$ to 5, a case where the magnetic field is dynamically important but not dominant. These simulations also show that it is important to include a realistic equation of state, including localized cooling or heating of the matter. Therefore it is expected that knowledge of the chemical composition, especially the species having a largest contribution to the thermal balance, will be included in future development of these investigations.

2.3.3 Circumstellar Disks

In the classical view of star formation [21, 26], young proto-stars are surrounded by an accretion disk, also called a circumstellar disk, which contributes to the feeding of the proto-star before it reaches its final mass. The so called class 0 proto-stars are deeply embedded and radiate mostly in the far infrared and sub-millimetre spectral range. At this stage, proto-stars are actively accreting, as testified by the presence of jets and molecular outflows. These outflows contribute to the release of energy and

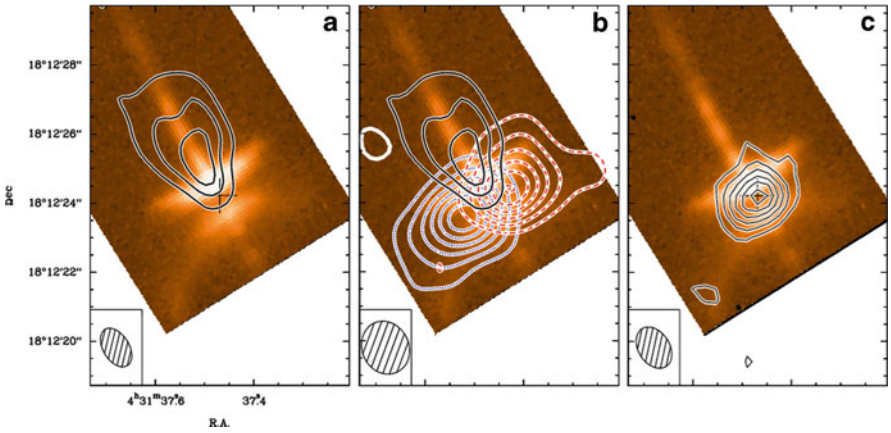

Fig. 2.3 The HH 30 system ([27]). The background image, taken with the Hubble Space Telescope (HST [28]), shows an edge-on disk traced by the *dark bar*, a jet perpendicular to the disk and scattered light from the embedded proto-star. The *left panel* presents the ^{12}CO($J = 2 \rightarrow 1$) emission at large positive and negative velocities relative to the dense core narrow emission. This high velocity ^{12}CO emission follows the narrow jet. The *middle panel* presents the ^{13}CO ($J = 2 \rightarrow 1$) emission in two velocity intervals indicated with *blue* and *red contours* for the emission approaching us/receding from us. This velocity pattern is consistent with Keplerian rotation around a solar mass star. The *right panel* presents the continuum emission due to dust grains in the circumstellar disk. The spatial resolution of the millimetre observations is $\sim 1''$ [27]

angular momentum outward that balances the losses of angular momentum and gravitational energy in the accretion process. However at this stage the presence of a Keplerian accretion disk is difficult to establish because most of the continuum and line radiation is associated with the dense core and the proto-stellar envelope. The presence of disks in the youngest proto-stars is therefore still debated.

Later stages in the proto-stellar evolution are called class I and class II, according to the accretion/ejection activity and the ratio of the total luminosity to the stellar luminosity, class II objects being more evolved, having a smaller accretion rate and a spectral energy distribution dominated by the proto-star radiation. Keplerian accretion disks are clearly present in class I and class II objects. In these objects, the spectral energy distribution becomes increasingly dominated by radiation from the (proto) stellar object, at visible and infrared wavelengths.

The presence of a disk can be detected in high angular resolution images, using adaptive optics systems or interferometers to reach sub-arcsec angular resolution (Fig. 2.3). These methods give access to the disk size, orientation and, coupled with spectroscopy, to its rotation pattern through the analysis of the variations of the line profiles with the position. An indirect detection of the presence of a disk can be established through analysis of the spectral energy distribution as the dust grains in the disk are significantly colder than the proto-star atmosphere and therefore produce an excess emission at longer wavelengths with respect to the close to black body radiation of the central object.

Circumstellar disks evolve together with their central object, becoming thinner and less massive through the combined actions of accretion onto the central object, and of dispersion of the disk triggered by the stellar radiation and winds/outflows. Dust grains evolve simultaneously with the gas: they settle to the disk mid-plane and start to grow in size through coagulation, first reaching centimetre sizes, and possibly up to boulder size or even larger objects. It is thought that planet embryos form at this period, which could start as early as 1 million years after the formation of the stellar embryo, and could last a couple of 100 million years. Planets gravitationally interact with their parental disk, creating density waves and gaps in the disk in which they evolve. This is especially true for the most massive ones that can radially migrate inward. The migration phenomenon is thought to be very common and also applies to the early phase of our solar system, as proposed in the so-called "Nice-Model" (e.g. [29] and references therein), in which the radial migration of proto-Jupiter and proto-Saturn led to a pronounced redistribution of the orbits of the small bodies, and could have caused an intense bombardment of the Earth and Moon surfaces.

While gas disks get rapidly dispersed, young stars and their planet embryos are still embedded in a tenuous disk of small dust particles continuously created during the frequent collisions of the large bodies (asteroids, comets, planet embryos, etc.). These dust disks are called "debris disks" to emphasize the fact that the dust does not originate from the ISM but is continuously replenished. The prototypical system surrounding the nearby star β Pictoris was discovered by the IRAS satellite (Fig. 2.4). It harbours an edge-on disk detected through the light scattered by the dust particles and extending up to hundreds of astronomical units. The small change in disk inclination between the inner and the outer regions has been interpreted as resulting from the gravitational interaction with a massive planet. This planet has been later discovered by high resolution imaging [30]. It may also cause the fall of comets/asteroids on to the star that were discovered earlier as variable absorption features in the visible stellar spectrum.

While β Pictoris is a young system (12 million years), with a relatively strong IR excess and bright scattered light emission from the disc, older systems like our Sun are still surrounded by a very faint dust disc. The study of proto-stars and their circumstellar discs, from the earliest phases of class 0 systems, to the debris discs, provides the necessary keys for understanding the formation and first evolutionary phases of our solar system. This is true for the dynamical evolution of the disc structure, as well as for the composition of the solid and gaseous matter. Conversely, information on the early evolution on the solar system, deduced from the analysis of the meteorites or from the study of the less evolved objects in the solar system, provides important constraints for understanding planet formation. It must be noted that the dynamical evolution of discs is closely related to the evolution of the solid and gaseous matter inside them. Dust grains provide shielding from the energetic radiation from the proto-star, and cold surfaces for freezing the volatiles like water, carbon monoxide, carbon dioxide, methanol, etc., onto grain mantles in the disk mid-plane. The presence of solid water is particularly important in the context of planet formation theory. Volatiles are more protected from the FUV

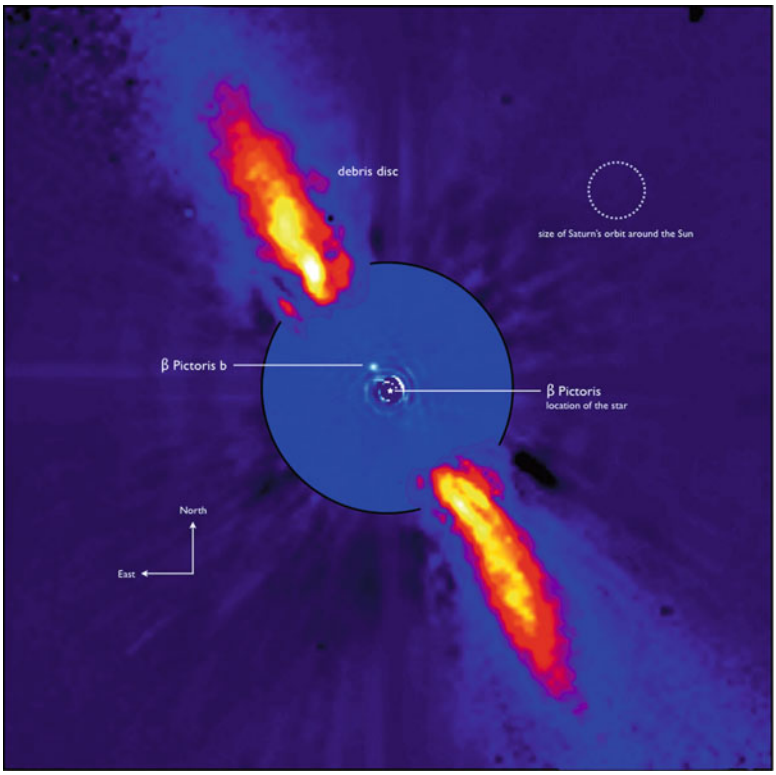

Fig. 2.4 The β Pictoris system in near infrared light. The faint reflected light radiation from the debris disc is revealed after a very careful subtraction of the much brighter stellar halo. The outer part of the image shows the dust disc, as observed in 1996 with the ADONIS instrument on the ESO 3.6 m telescope; the inner part of the image has been obtained with the NACO instrument on the ESO Very Large Telescope. The newly detected source is more than 1,000 times fainter than β Pictoris, aligned with the disc, at a projected distance of eight times the Earth-Sun distance. Both parts of the image were obtained on ESO telescopes equipped with adaptive optics [30]

radiation in grain mantles than in the gas phase, hence an active organic chemistry can proceed in the ice mantles, possibly forming the first building blocks of the organic species detected in comets and meteorites. The study of circumstellar discs in the context of planet formation is a very active field of research. Because circumstellar discs are relatively small objects a few arcsec across (Fig. 2.3), especially their inner region where planets form, the knowledge of the disk chemical composition is currently limited to the strongest spectral features available. With the upcoming of more powerful instruments, in terms of sensitivity and angular resolution like ALMA, VLT and soon E-ELT, tremendous progress is expected in the near future.

2.3.4 Photodissociation Regions and Shocks

Energy is fed in the interstellar medium either through impinging radiation from the surrounding stars or through stirring the gas by dynamical processes. Therefore, it is very important to understand (1) the coupling of matter with radiation on the one hand, and (2) the specific chemistry induced by shocks. In both cases, the modelling must involve the description of the heating and cooling processes of matter, which requires a detailed understanding of the relevant physical and chemical processes controlling the composition, electron fraction and thermal balance.

In addition, the modelling must include a macroscopic description of the system in consideration, its geometry, and the associated physical conditions.

The name "Photodissociation regions" or "PDRs" refers to the illuminated edges of dense molecular gas as well as the lower density diffuse and translucent interstellar medium, as both environments are bathed by far ultraviolet photons. One of the most famous examples, the edge of the horsehead nebula is illustrated in Fig. 2.5. In such regions the heating is dominated by the interaction of these far ultraviolet photons with matter, especially with the dust grains through the photoelectric effect. Indeed, FUV photons can eject an electron from an inner shell of an atom bound in a dust grain. This energetic electron with typically 1 eV of kinetic energy, subsequently heats the gas by colliding with other particles. The process is most effective for small dust grains, like the PAHs and very small grains. The cooling is dominated by radiation of abundant species in the gas phase such as atomic oxygen **OI**, ionized carbon **CII**, $\mathbf{H_2}$ and CO (Table 2.2). FUV photons also have a profound influence on the gas composition and on the dust structure. As the ionization energy of carbon is lower than that of hydrogen, ionized carbon is present in the neutral gas and can participate in the chemistry, contributing to the formation of many carbon bearing species. FUV photons can also induce the desorption of species frozen onto grain mantles, contributing to the destruction of these mantles and the release of frozen molecules into the gas phase. Finally molecules are destroyed by photons. During the destruction process, molecules can access excited states that produce specific emission lines. This is especially true for molecular hydrogen, H_2, whose photodissociation involves absorption involving its electronic transitions. The excited H_2 molecule can either dissociate or be de-excited through line emission and collisional de-excitation. The former process destroying H_2 is relatively inefficient, with radiation being preferred to dissociation in about 90% of the cases. The line emission produced during the de-excitation process can be detected in the near infrared (e.g. Fig. 2.5) and used as a clean probe of the interaction of FUV radiation with molecular gas.

State of the art models of photodissociation regions today involve hundreds of chemical species, thousands of chemical reactions, and tens of physical and chemical processes in order to accurately describe the physical and chemical structure of a piece of gas illuminated by FUV photons. This degree of sophistication cannot yet be implemented in 3D dynamical models. Most PDR models are therefore steady-state and one dimensional, with ongoing developments towards simplified three

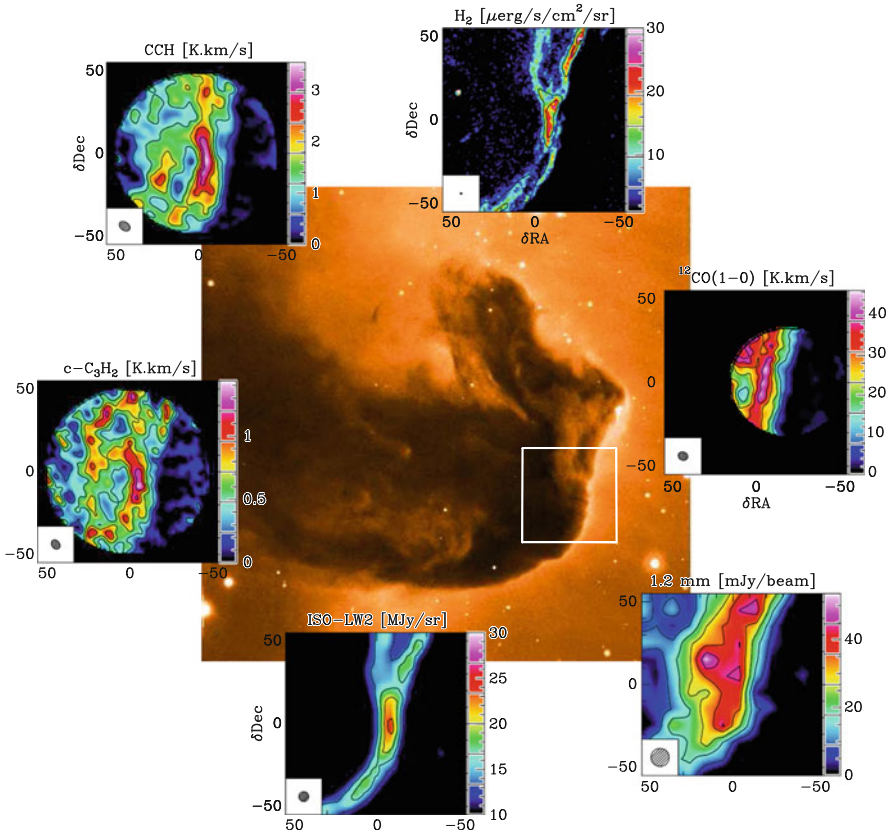

Fig. 2.5 The horsehead nebula, a dark cloud illuminated on its right edge by FUV radiation from the nearby O9 star σOri. This edge is a template source for studying the physical and chemical processes in UV irradiated interstellar matter. The background image is taken in the visible at ESO. The *small colour* pictures show the distribution in various spectroscopic tracers [31]

Table 2.2 Main gaseous cooling lines

Species	Transition	Wavelength/μ*m*	T/K
H_2	Rotational lines	28, 17, 12, 9.3	200–1,000
Oxygen [OI]	Fine structure	63, 145	100–400
Ionized carbon [CII]	Fine structure	158	50–300
Neutral carbon [CI][a]	Fine structure	610, 370	20–100
CO[b]	Rotational lines	124–2,600	10–200
H_2O[c]	Rotational lines	538– ~60	50–500

[a]Weaker contribution compared to [CII].
[b]Stronger contribution than [CI], saturated lines.
[c]More important in shocks than in PDRs.

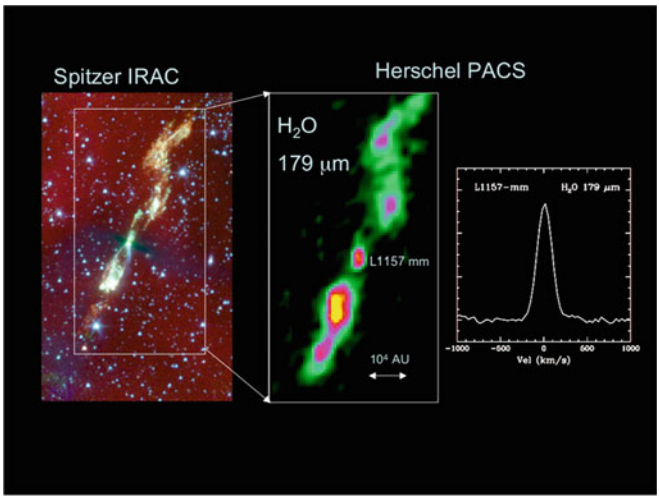

Fig. 2.6 The molecular outflow created by the class 0 proto-star L1157 viewed in the infrared by the Spitzer (*left*) and in the far infrared with Herschel (*right*) satellites. The Spitzer image taken with the IRAC camera is dominated by emission from the rotational lines of H_2. The Herschel image taken with the PACS instrument at 179 μm, the wavelength of one of the strongest lines of water vapour ($2_{1,2} - 1_{0,1}$) shows the excellent agreement between the H_2 and water vapour morphology [35]

dimensional geometries. The PDR code developed in the Meudon Observatory [32] is accessible on line (http://pdr.obspm.fr). It is however possible to implement a very coarse treatment of the chemistry and the interaction of matter with radiation in magnetohydrodynamic (MHD) simulations. The Heidelberg team has published pioneering results, showing the interplay of chemistry and dynamics clearly [33]. While both approaches have their pro and cons, it is foreseeable that they will be more often combined in the near future, thanks to a rapid increase in computer capabilities and the development of more advanced numerical codes.

Shocked regions are relatively frequent in the interstellar medium. Among the main shock sources are the jets from young stars creating molecular outflows (Fig. 2.6), and the shocks induced by supernovae explosions the most studied. The latter shocks can reach very large velocities, up to 100 km s^{-1} or higher, and have typical speeds of a few tens of km s^{-1}. Slower shocks are also present, as consequences of the large scale streaming motions along the spiral arms, stirring of the interstellar medium by stellar winds, distant supernovae shocks, and resulting turbulent motions. Understanding the shock physics is therefore as important as understanding the PDR physics for a global description of the interstellar medium. Because the interstellar medium is penetrated by magnetic fields, the shock structure can be very different from pure hydrodynamical shocks. As explained in the review by Draine and Mc Kee [34], in relatively slow shocks, a magnetic precursor is formed ahead of the shock, that informs the gas upstream as to the arrival of the shock. As the ionization fraction is very low, less than 10^{-7} in shielded molecular

gas, the ionized and neutral fluids are decoupled by this magnetic precursor, with the neutral fluid being essentially unaffected while the ions are accelerated and heated. This decoupling induces a velocity drift between the ions and the neutrals, which leads to a delayed acceleration and heating of the neutrals through the ion-neutral friction. Since the gas can cool at the same time, the overall velocity and density pattern remains continuous in the shock reference frame. These shocks are therefore labelled "C-shocks" for "Continuous shocks". When the shock velocity becomes too large, the magnetic precursor cannot play its role and the shock becomes discontinuous as a pure hydrodynamical shock. These shocks are labelled "J-shocks" with "J" referring to the presence of "Jumps". This description is very schematic. In realistic cases, shocks may not be stationary, and have a more complex morphology than the ideal case of a one-dimensional shock front with the magnetic field oriented perpendicular to the shock front. For a more complete introduction to PDR and shock physics, the reader is invited to consult specialized references such as [34].

2.4 Constituents of the Interstellar Medium

The analysis of radiation across the electromagnetic spectrum has allowed astronomers to uncover the composition of the neutral interstellar medium, its spatial variation and how it relates to the local environment (physical conditions) as well as the overall evolutionary stage of the object.

2.4.1 Neutral Gas

Table 2.3 presents a summary of the molecules detected in the interstellar medium or in the envelope of evolved stars, most notably the bright carbon star **IRC +10216**. Species in which a hydrogen atom has been substituted by a deuterium atom are listed as well, as they are extremely valuable tools to understand the chemical evolution of the star-forming interstellar matter. The list has been established using on line data bases such as the Cologne Data base for Molecular Spectroscopy (CDMS http://www.astro.uni-koeln.de/cdms/molecules), the splatalogue (http://www.splatalogue.net) and The Astrochymist (http://astrochymist.org/).

This list has been obtained through dedicated observations across the electromagnetic spectrum, from the far ultra violet for H_2 or N_2, down to centimetre wavelengths for NH_3 or HI. The most effective detection method is the analysis of the rotational spectrum of molecules, in the centimetre to sub-millimetre wavelength spectral range because extremely sensitive detectors are available with high spectral resolution capabilities. However, this method is biased towards species with a permanent electric dipole moment that allow the efficient emission (or absorption) of rotational lines (see Chap. 1). Symmetrical species like N_2, C_2 and alike cannot be

Table 2.3 List of detected interstellar and circumstellar molecules, radicals and ions, grouped by the number of atoms (***N***) they contain. Species detected with UV, visible or infrared spectroscopy are indicated in italics

N	Observed species
2	*H_2*, *H D*, OH, O_2, OH^+, CH, CH^+, NH, HF, HCl, SH, SH^+, CO, CO^+ CS, SO, SO^+, SiO, *C_2*, CF^+, NO, O_2, PN, SiS, *N_2*, HCl^+, SiC, AlF, AlCl, NaCl, KCl, SiN, CP, PO, AlO, CN^-
3	*H_3^+*, *C_3*, C_2H, C_2O, C_2S, HCO, HCO^+, HOC^+, CH_2, O_2H_2O, H_2O^+, NH_2, HCN, HNC, HCS^+, H_2S, N_2H^+, OCS, SO_2, CO_2, HNO, N_2O, H_2Cl^+, MgCN, MgNC, NaCN, *c*-SiC_2, SiCN, AlNC, SiNC, HCP, CCP, AlOH, KCN, FeCN, O_2H
4	NH_3, H_3O^+, *C_2H_2*, H_2CO, *CH_3*, $HCNH^+$, H_2CN, H_2CS, HC_2N, *c*-C_3H, *l*-C_3H, C_3O, C_3S, *l*-C_3H^+, C_3N, HNCO, HOCN, HCNO, HNCS, HSCN, $HOCO^+$, HOOH, *c*-SiC_3, C_3N^-, PH_3
5	H_2C_2O, *C_5*, C_4H, C_4H^-, *c*-C_3H_2, *l*-C_3H_2, H_2CCN, *CH_4*, HC_3N, HC_2NC, HNC_3, HC_2NH, HCOOH, NH_2CN, H2COH^+, HCOCN, C_4Si, SiH_4
6	CH_3OH, C_5H, *l*-H_2C_4, *C_2H_4*, CH_3CN, CH_3NC, CH_3SH, HC_3NH^+, HC_2CHO, NH_2CHO, *c*-H_2C_3O, C_5N, C_5N^-, *l-HC_4H*, *l*-HC_4N, H_2CCNH
7	C_6H, C_6H^-, CH_2CHCN, CH_3CCH, HC_5N, CH_3CHO, CH_3NH_2, *c*-C_2H_4O, H_2CCHOH
8	CH_3C_3N, HC(O)OCH_3, CH_3COOH, CH_2OHCHO, C_7H, H_2C_6, *l-HC_6H* CH_2CHCHO, CH_2CCHCN, NH_2CH_2CN
9	CH_3C_4H, $(CH_3)_2O$, C_8H, C_8H^-, CH_3CH_2CN, CH_3CH_2OH, HC_7N, CH_3CONH_2, C_3H_6
10	CH_3C_5N, $(CH_3)_2CO$, $(CH_2OH)_2$, CH_3CH_2CHO
11	HC_9N, CH_3C_6H, C_2H_5OCHO
12	*C_6H_6*, $CH_3OC_2H_5$(?), C_3H_7CN
$\geq$ 13	$HC_{11}N$, *C_{60}*, *C_{70}*
	Deuterated species
2	HD, ND
3	H_2D^+, D_2H^+ HDO, D_2O, HDS, D_2S, DCN, DNC, DCO^+, N_2D^+
4	NH_2D, ND_2H, ND_3, HDCO, D_2CO, HDCS, D_2CS, *c*-C_3D
5	C_4D, *c*-C_3HD, DC_3N
6	CH_2DOH, CD_2HOH, CD_3OH, CH_3OD, CH_2DCN

detected through their pure rotational pattern although they can be very abundant. When a suitable bright background source is present, absorption spectroscopy either in the UV-visible (searching for the electronic transitions of the molecules) or in the infrared (aiming at the vibrational transitions) can be performed. Because of the limited number of suitable sources, the weakness of the vibrational transitions, and lower spectral resolution, the number of species accessible through these techniques is restricted to relatively abundant species. Furthermore, it is important to note that the chemical composition is closely related to properties of the environment. All molecules listed in Table 2.3 will not be present in a single source. Some species like CO are widely present, while others like SiO are formed in specific events and can be used to locate these events. The analysis of the chemical composition of a given source therefore provides most of the clues on its structure, gas column density, gas density, electron fraction, magnetic field as well as its dynamics, through the analysis of the detected spectral lines.

Among the molecules detected so far in the interstellar medium, some species have been more widely used than others as physical and chemical probes. Some of the more commonly used species are described below. This choice is somewhat subjective and care must be taken when analysing molecular spectral lines, to compare with detailed physical and chemical models before drawing definitive conclusions.

2.4.1.1 Density and Temperature Determination

The local gas density cannot be directly measured as detected signals always are integrated along the line of sight. However it can be deduced from analysis of the degree of excitation of molecules, i.e. from the comparison of populations of different energy levels, which results from competition of radiative and collisional excitation and de-excitation (see Chap. 1). The most abundant collision partner is molecular hydrogen H_2. Collisions with hydrogen and helium atoms, and with electrons, can also be important especially in diffuse regions. The role of collisional excitation is best illustrated with the notion of critical density n_{cr}, which corresponds for a given molecular transition to the minimum gas density for exciting the molecule and producing an emission line. For a two level system at temperature T, and assuming H_2 as the sole collision partner, the balance between collisional excitation and emission of radiation can be written:

$$n_u A_{ul} + n_u n(H_2) C_{ul} + n_u I_\nu B_{ul} = n_l n(H_2) C_{lu} + n_l I_\nu B_{lu} \tag{2.1}$$

where n_u and n_l refer to the populations in the upper and lower energy levels of the system, A_{ul} and B_{ul} are the Einstein coefficients for spontaneous and induced emission, C_{lu} and C_{lu} the collisional rates for excitation/de-excitation, $n(H_2)$ the gas density and I_ν the local radiation intensity. The transition frequency ν is related to the energy level as

$$\nu = (E_u - E_l)/h \tag{2.2}$$

and the total number of molecules n_{mol} is $n_l + n_u$. The detailed balance implies,

$$C_{ul}/C_{lu} = B_{ul}/B_{lu} = g_l/g_u e^{(E_u - E_l)/k_B T} \tag{2.3}$$

Therefore equation (2.1) can be rewritten, neglecting the radiative coupling terms:

$$n_u/n_l = 1/((A_{ul}/n(H_2)C_{ul}) + (g_l/g_u)e^{h\nu/k_B T}) \tag{2.4}$$

This formula shows that when the collisions are frequent, the first term in the denominator becomes small compared to the radiative de-excitation, and the level populations approach thermodynamic equilibrium at the kinetic temperature T,

namely $n_u/n_l = g_u/g_l \; e^{-h\nu/k_B T}$. On the contrary, when the de-excitations are dominated by radiative processes, the population in the upper level is very small and $n_u/n_l \sim n(H_2)C_{ul}/A_{ul}$. The change of behaviour occurs close to the critical density defined as $n_{cr} = A_{ul}/C_{ul}$. This concept can be used for multilevel systems, using the balance between the various excitation and de-excitation routes. The concept of critical density is useful for determining the order of magnitude of the gas density probed by a given molecular transition.

Ammonia (NH_3) and formaldehyde (H_2CO) are among the best species for probing the physical conditions as they have many accessible lines coupling levels of different excitation energies, and their collisional cross sections have been accurately computed [36, 37].

The kinetic temperature cannot be directly measured from the observations but can be deduced from the analysis of the line profiles and molecular excitation as the level populations are also sensitive to the temperature. For an accurate determination of the physical conditions, including the kinetic temperature, the full set of the statistical equilibrium calculations must be solved. There are some freely available numerical codes, such as RADEX ([38], http://www.strw.leidenuniv.nl/moldata/radex.html). They make use of extensive data bases of collisional cross sections, LAMDA (Leiden Atomic and Molecular DAtabase http://www.strw.leidenuniv.nl/moldata/), and BASECOL (http://basecol.obspm.fr/), that are now part of the European initiative VAMDC (Virtual Atomic and Molecular Data Center http://www.vamdc.eu/).

2.4.1.2 Ionization

The ionization fraction is an important parameter of the physics of the interstellar medium, as it controls the gas coupling with the magnetic fields. Because the main charge carriers are electrons, they are not directly accessible through spectroscopy and other methods must be used to probe the total ion content. The most common methods take advantage of the variations of the chemical composition of the gas as a function of the ionization fraction, and involve measurement of the abundances of different molecular ions (e.g. HCO^+, HOC^+, N_2H^+) or radicals (e.g. atomic carbon) that are particularly sensitive to the presence of electrons. The key point in these methods is the necessity to understand thoroughly the processes regulating the abundances of these molecular ions to be able to accurately extract the dependency on the ionization. For instance [39] discuss the variation of the ionization fraction across the edge of the horsehead nebula.

A related issue is the determination of the ionizing rate of the neutral gas produced by cosmic rays ζ. These energetic particles have a very long mean free path and can travel far from their birth place. They can ionize atomic and molecular hydrogen forming H^+ and $H_2{}^+$ respectively. $H_2{}^+$ rapidly reacts with molecular hydrogen to form the more stable ion $H_3{}^+$. Since H and O have almost identical ionization energies of 13.598 eV (H) and 13.618 eV (O) H^+ can transfer its charge to atomic oxygen, forming O^+ that reacts with molecular hydrogen to form OH^+. Then

other hydrogen abstraction reactions lead to H_2O^+ and $\mathbf{H_3O^+}$. H_3^+, and possibly the oxygen ions, can be therefore be used as probes of the cosmic ray ionization rate ζ [40, 41].

2.4.1.3 Magnetic Field Measurement

As explained below, magnetic fields induce a small modification of the energy levels of molecules, through the Zeeman effect, which is particularly important for paramagnetic species like O_2 or SO, or radicals with an unpaired electron like CN, CCH or OH. With the typical strength of interstellar magnetic fields, from a few tens to a few hundreds μGauss, the signature of interstellar magnetic fields in the line profile is very weak and difficult to separate from other effects leading to deformations of the line profiles, especially systematic instrumental effects. In order to calibrate the instrumental effects, molecular species exhibiting hyperfine transitions with different sensitivities to the magnetic fields such as CN are usually preferred for probing the magnetic field intensity (see Crutcher [42] for a review).

2.4.1.4 Tracers of Astrophysical Environments

Because the chemical composition is highly dependent on the present and past physical conditions, it is possible to use some species, or some spectral lines as tracers of specific environment. As for the ionization fraction, the definition is somewhat subjective, hence the applicability of the tracers listed below to a new dataset must be carefully compared with both theoretical models and previous observations. Because the subject is evolving fast, the list of tracers presented below must be viewed as incomplete.

PDR Tracers

Photodissociation regions (PDRs) are defined as regions where the chemistry is dominated by photons. Hence the chemistry of PDR tracers must be dominated by photo-induced processes, at least indirectly. Reactive species, rapidly destroyed by reactions with H_2 or abundant neutrals are therefore good tracers of the illuminated outer layers of molecular clouds. The list includes the gas coolants [CII], [OI] and [CI], radicals like HCO, CCH or c-C_3H_2, as well as reactive ions like CO^+, HOC^+ or CF^+. The rotational and rovibrational lines of H_2 are also bright in PDRs.

Shock Tracers

Good shock tracers must show the highest abundance contrast between the ambient medium and the shocked gas. Because most of the silicon is locked up in grain

cores, the SiO abundance is very low in the interstellar medium, except in shocked regions where sputtering of some silicated materials from the grains leads to the release of silicium and the formation of SiO. A similar story can be told for water vapour, which is locked up in grain mantles as solid ice and released in the gas phase in shocks. Other shock tracers can involve abundant species in grain mantles like methanol (CH_3OH) but their signature is not as clear as those of SiO and H_2O because the methanol abundance of the quiescent gas is not negligible. Finally, shocks are also bright sources of H_2 emission because of strong gas heating in the shocks.

Tracers of Turbulent Dissipation Regions

The presence of reactive ions like CH^+ in the diffuse interstellar medium has been a challenge for interstellar chemistry since CH^+ is easily destroyed by reactions with H_2 but slow to form under the known physical conditions of the diffuse interstellar medium. It now appears that a "warm chemistry" can develop in the tiny dissipative structures of the interstellar turbulence, enabling the formation of transient species like CH^+ and SH^+ [43]. The opening up of the sub-millimetre sky by the Herschel telescope has led to the discovery of several new reactive ions, enabling a better characterization of their chemistry. In the future, these tracers should bring interesting constraints on the properties of the interstellar turbulence.

Cold Cores

With their larger density compared to the background, and the cold grain temperatures, dense pre-stellar cores appear as bright sub-millimetre sources. A specific chemistry develops at the cold temperatures and high densities. While the main molecular species like CO freeze onto dust grains because of the very low grain temperatures ($\sim$10 K), the chemistry remains active. In particular, the cold temperatures are particularly favourable for enhancing the deuterium fractionation, with observed abundance ratios of the deuterated species compared to the main isotopologue larger than one tenth, while the elemental abundance of deuterium relative to hydrogen is 20 ppm. The presence of multiply deuterated species with up to three D atoms is another key characteristic of pre-stellar cores. This includes the deuterated forms of H_3^+ [18], Hence the presence of strong rotational lines from deuterated molecular ions (H_2D^+, DCO^+, N_2D^+) can be used to locate cold dense cores. The abundances of deuterated molecular ions is sensitive to the temperature because the fractionation is induced, in the gas phase, by the exothermic reaction between H^+ and HD:

$$H_3^+ + HD \rightarrow H_2D^+ + H_2(\Delta E = 232K) \qquad \text{(R2.1)}$$

At the low temperatures of cold dense cores, the rate of the forward reaction is much larger than the rate of the reverse reaction, and the deuterium fractionation is favoured. The fractionation is limited by the H_2D^+ destruction processes, namely the dissociative recombination with electrons and reactions with neutral species (CO, N_2, etc.) that destroy H_2D^+ and H_3^+ faster than the reaction with HD. Similar reactions with D_2H^+, D_3^+, CH_2D^+ must also be considered in chemical networks, all contributing to deuterium enrichment.

In addition to deuterated species, some nitrogen bearing species can also be used to study the properties of cold dense cores, notably NH_3 and N_2H^+ [26] as emission maps show that they are spatially associated with the cold dense cores. Indeed, in time dependent models, these species need a rather long time to reach their steady state abundance which may explain this spatial association.

Hot Cores and Hot Corinos

The chemical composition of hot cores and hot corinos is much richer than at any other place in the interstellar medium. In particular, a huge variety of organic species can be detected in these warm and compact objects, such as CH_3OH, $HCOOCH_3$, CH_3CN, $(CH_3)_2O$. At the warm temperatures created by strong heating by the newly formed stars, ice mantles can evaporate, liberating in the gas phase the frozen molecules and simultaneously triggering a rich chemistry. Therefore many of the polyatomic species listed in Table 2.3 are only found in hot cores and hot corinos. As the chemical time scales associated with the processing of different abundant ices are different, high spatial resolution studies have shown that oxygen bearing species may show a different spatial pattern than nitrogen bearing species in some cases. Two sources stand out among the known hot cores, the hot core in the Orion KL region, close to the infrared source IRc2 because of its small distance (400 pc), and the "large molecule heimat" in the SgrB2 molecular complex because of the high abundance of organic species. The class 0 proto-star IRAS 16293-2422 (Fig. 2.2) is considered as a prototype of hot corino. We recall that the main difference between hot cores and hot corinos is the association with high mass stars for hot cores, and with low to intermediate mass stars for hot corinos. Furthermore, deuterated saturated molecules, like D_2CO are usually more abundant in hot corinos than in hot cores [21].

2.4.2 Dust Grains

2.4.2.1 Composition

The physics of dust grains is a vast topic that is only briefly introduced here as other chapters in the book present chemical aspects. The term "dust grains" refers to the solid particles present in the interstellar medium (Fig. 2.7) as well as in

Fig. 2.7 Image of a fraction of the Rosette nebula obtained at far infrared wavelengths with the Herschel telescope. The *colours* correspond to the three monochromatic images that have been combined, with *blue coding* for the shortest wave- length (60 μm) and *red* for the longest wavelength (500 μ*m*) [45]. Regions with the warmest dust appear in *blue* while the cold dust regions, further away from the heating sources, appear in *red*

circumstellar disks, proto-planetary and debris disks, as well as in evolved star envelopes. These sub-micronic solid particles are mainly formed in the last evolutionary phases (Red Giant phase and beyond) of stars, and possibly in other more energetic events (e.g. supernovae shocks). The diversity of progenitors leads to a diversity in the dust grain materials, grouped in two main categories, silicate grains and carbonaceous particles (Table 2.4).

In the interstellar medium, the mass of solid particles is about one hundredth of the total mass of the gas. The composition of interstellar dust grains can be established using several sources of information. By comparing the elemental abundances in the sun and in nearby stars with those in the interstellar medium, it is possible to identify the elements showing a deficit in the gas, because they are locked in solid particles. For instance gas phase abundances of silicon, magnesium and iron is lower by more than one order of magnitude in the diffuse interstellar medium than in the sun, because silicon is mostly locked up in solid silicate particles that also include some magnesium and iron. By contrast, gas phase abundances of sulfur and nitrogen are very similar in the sun and in the diffuse interstellar medium indicating that these elements do not contribute much to the building of solid particles in this environment.

Another source of information is the analysis of the preserved dust grains in meteorites. Indeed, some meteorites contain grains that can be identified through their isotopic compositions as being formed before the birth of the solar system. These "pre-solar grains" carry interesting information on the formation places of dust grains, and on their possible composition. In addition to silicates and oxides, one important component of pre-solar grains in primitive meteorites (carbonaceous chondrites) is nanodiamonds (size $\sim$2 nm).

Table 2.4 Composition and properties of interstellar dust grains

Category	Material	Size	Main bands
Amorphous silicates[a]	Pyroxene ($Mg_x\ Fe_{1-x}\ SiO_3$)	$\sim$0.1 μm	9.7, 18 μm
	Olivine ($Mg_x\ Fe_{1-x}\ SiO_4$)		
Oxides	SiO_2, MgO, Fe_3O_4, etc.		
Carbon material	Amorphous carbon	$\sim$10 nm	3.4 μm
	Graphite[b]	$\sim$10 nm	2175 Å
	PAHs[c]	$\sim$1 nm	3.3, 6.2, 7.7, 8.6, 11.3 μm
Ice mantles[d]	H_2O		3.07, 6.0 μm
	CO		4.67 μm
	CO_2		4.27, 15 μm
	CH_3OH		8.5, 3.9, 8.9, 9.65 μm

[a]Most silicates are amorphous. Crystalline silicates have been identified through their infrared spectral features in sources where they form (see text).
[b]Assignment debated between graphite and possibly PAHs and cluster of PAHS (see text).
[c]Polycyclic Aromatic Hydrocarbon (e.g. coronene $C_{24}H_{12}$).
[d]Ice mantles are mixtures of several components, only the most abundant ices are listed. See e.g. [44] for a more complete list of ice constituents.

Finally, information on the composition, size and quantity of solid material can be extracted from analysis of the spectra of interstellar sources. Dust grains are the main sources of reddening in the UV/visible and near infrared spectral regions, and contribute most of the sub-millimetre continuum radiation through their thermal emission. Several spectral bands due to solid materials have been found in the spectra, leading to important information on their size and composition (Table 2.4). The information listed in Table 2.4 must be viewed as a short summary of a complex topic. For instance the size distribution of dust grains extends from nanometre particles up to nearly micron size solids in the variety of interstellar environments, and could extend to even larger particle sizes in proto-planetary disks. The profile of the silicate absorption band at 9.7 μm indicates that the grains responsible for this absorption are composed of amorphous silicates, in contrast with the nature of solar system grains that show both crystalline and amorphous components. Crystalline silicates are relatively easy to detect since they have a richer band spectrum than amorphous silicates, with bands specific of each material. The ISO satellite, followed by the Spitzer Space Telescope, discovered the presence of crystalline silicates in some circumstellar disks as well as in the ejecta of red giant stars where these particles form. Therefore, the physics of silicate grains is not as simple as initially thought, as it now appears that these particles continuously evolve, possibly through the combined effect of energetic radiation, cosmic ray particles, collisions and shocks.

The carbonaceous grain population, including polycyclic aromatic hydrocarbons (PAHs) and fullerenes is of particular interest for astrochemistry. They account for at least 10% of the total carbon content and can contribute up to $\sim$20% of the total infrared luminosity of a star forming galaxy. The PAH family has been identified

through strong vibrational bands in the infrared (notably at 3.3, 6.2, 7.7, 8.6 and 11.3 μm, see Fig. 1.4), that indicate that this population is ubiquitous, in the interstellar medium as well as in external galaxies up to very large redshifts (see the book by Joblin and Tielens [46] for a presentation of the recent results on PAHs). Although no single molecule has been identified so far, the combined work on observations, laboratory experiments and theory has enabled this population to be better defined. It is now believed that PAHs exist in the diffuse ISM and can be either neutral, positively or negatively charged. Their sizes range from a few tens to a few hundreds of carbon atoms. In dense gas, shielded from the FUV radiation, PAHs are thought to aggregate forming PAH clusters of several hundreds of carbon atoms. Fullerenes have been recently detected in the ISM and circumstellar envelopes but these symmetrical particles contain a smaller fraction of the carbon, at the percent level.

2.4.2.2 Physics

Dust grains play an important role in the physics of dense interstellar gas. When irradiated by far ultra violet photons, dust particles can get positively charged by the ejection of an energetic electron with typically 1 eV kinetic energy, through the photo-electric effect. This energetic electron loses its energy by collisions with gas species, and hence heats the gas. Since the effect is most efficient for small particles that have the largest surface area to volume ratio, the small carbonaceous dust particles and the PAHs are the most efficient dust particles for this heating mechanism. Although the efficiency is only a few percent, the photo-electric effect is one of the most important heating mechanisms of the gas since it allows transfer of energy from radiation to matter.

Dust grains can also contribute to the thermal balance as they efficiently cool through their thermal emission. At low densities the gas and grain temperatures are different since the gas cools less efficiently than the dust. However, for gas densities greater than about 10^5 cm^{-3}, collisions enable an efficient coupling between the gas and dust particles, leading to similar temperatures. Depending on the difference in temperatures, these collisions can be considered as either a cooling or a heating mechanism.

Because they are subject to photo-electric heating, dust grains usually carry charges, and therefore contribute to the charge balance. It is important to know the charge on dust grains since the efficiency of the photoelectric effect heavily depends on the grain charge, the ejection of an electron being more difficult from a positively charged grain than from a neutral particle. In addition grains can contribute to the neutralization of charged particles. Their role in the charge balance is especially important in the dense and well shielded regions where the ionization fraction is low since they can help to maintain a coupling of matter with the magnetic field.

Another key role of dust grains is their role in the formation of molecular hydrogen. Except in the very early universe, the formation of H_2 on dust grains is

significantly more efficient than a pure gas phase route. First deduced from the comparison of measurements of H and H_2 column densities with a simple model [47], the formation of H_2 on solid surfaces is now the subject of laboratory and theoretical studies that are subsequently used in chemical models [48]. The newly formed H_2 is released with excess energy corresponding to a fraction of the binding energy of H_2 (4.5 eV). Therefore the formation of H_2 contributes to the heating of the gas.

2.4.2.3 Chemistry

Dust grains act as small chemical reactors. They also participate in the circulation of matter through the various phases of the interstellar medium. Ice mantles built up on silicate grains in dense cores, both through condensation of gas phase species and through additional processing in the solid phase. Because the molecules are closer to each other in ice mantles than in the gas phase, the chemistry can be more efficient in ice mantles. Started with difficult observations from the ground, the inventory of ice mantles has fully benefited from the ISO and Spitzer missions, with their sensitive spectrometers fully covering the infrared spectral domain [44]. This field has fully benefited from the synergy between astrophysical observations and laboratory experiments, where the formation and evolution of interstellar ices can be studied. The excellent agreement of the infrared spectra of material produced in the laboratory with astrophysical data indicates that the most important features are well understood. The effort is now put into understanding the physical and chemical processes leading to the complex ice composition when starting with relatively simple ice mixtures (e.g. [49]).

Indeed, one of the most important roles of dust grains is the production of complex organic molecules in grain mantles, which would not be possible through pure gas phase chemistry. The detection of organics such as those listed in Table 2.3 in hot cores and hot corinos with radio telescopes shows the chemical richness produced in ice mantles, both during the cold pre-stellar phase and during the warm-up phase following the birth of the proto-star(s). The energetic radiation associated with young proto-stars, with intense FUV and X-Ray emission, likely contributes to the processing of the ice mantles and helps in building complex organics. The detection through radio techniques is biased towards polar species, with radio spectra strong enough to be identified. It is likely that the inventory of organics in astrophysical ices is significantly richer than those identified so far.

The analysis of the soluble organic matter of primitive meteorites provides interesting clues on this issue, since this material has condensed in the primitive nebula in an analogous way as ices condense in dense interstellar clouds. The processing induced by the radiation of the young sun is also similar to that expected in the ISM. The composition of the soluble organic matter is very rich, with numerous amino-acids. The direct detection with high spectral resolution techniques of a particular amino-acid is extremely difficult since the expected spectrum in the astrophysical sources will be composed of a very large number of weak spectral features that may

not be individually detectable. A better approach is probably to focus on laboratory experiments to learn more about the possible routes to chemical complexity in space. For instance, [50] have recently detected in ice residues a key intermediate species in the synthesis of peptides, hydantoin, confirming the important role of ice mixtures in the synthesis of complex organics.

2.5 Observations of the Dense Interstellar Medium

The properties of the interstellar medium have been deduced from analysis of extensive observations covering most of the electromagnetic spectrum (Fig. 2.8). Except for the analysis of pre-solar grain inclusions in meteorites, no in-situ measurement is possible because of the large distance of the objects. In the following, we describe the main observation methods and the information carried out by photons across the electromagnetic spectrum.

2.5.1 Photometry

For an extended object like the interstellar medium, imaging is a natural source of information, providing clues on the spatial structure, geometry and many other physical properties depending on the wavelength of interest.

2.5.1.1 Visible and Near Infrared

Images in the visible and UV are dominated by the combination of scattering and absorption of the radiation from surrounding and embedded stars. Strong visible lines, as those of hydrogen (Hα at 656.3 nm) can also contribute to the detected flux. Scattering and absorption are produced by the dust grains, and are therefore used to study the dust grain size distribution and composition. Both effects cause a dimming of stellar radiation which varies as a function of wavelength and is more pronounced at short wavelengths. The variation of the extinction as a function of wavelength is called the extinction curve. It decreases continuously from the FUV to IR wavelengths, except for the "extinction bump" at 217.5 nm. Dense regions of interstellar clouds have a large enough column density of dust grains that the light from the stars in their background is totally dimmed and they appear as black patches in the bright trail of the Milky Way. The first catalogues of so-called "dark clouds" were therefore established in the beginning of the twentieth century, by e.g. Barnard and co-workers. Barnard 68 (Fig. 2.1) is a good example of such dark clouds. Because the extinction decreases at near infrared wavelengths, background stars that are totally invisible in the optical can be detected in the near infrared J (1.2 μm), H (1.6 μm) and K (2.1 μm) bands.

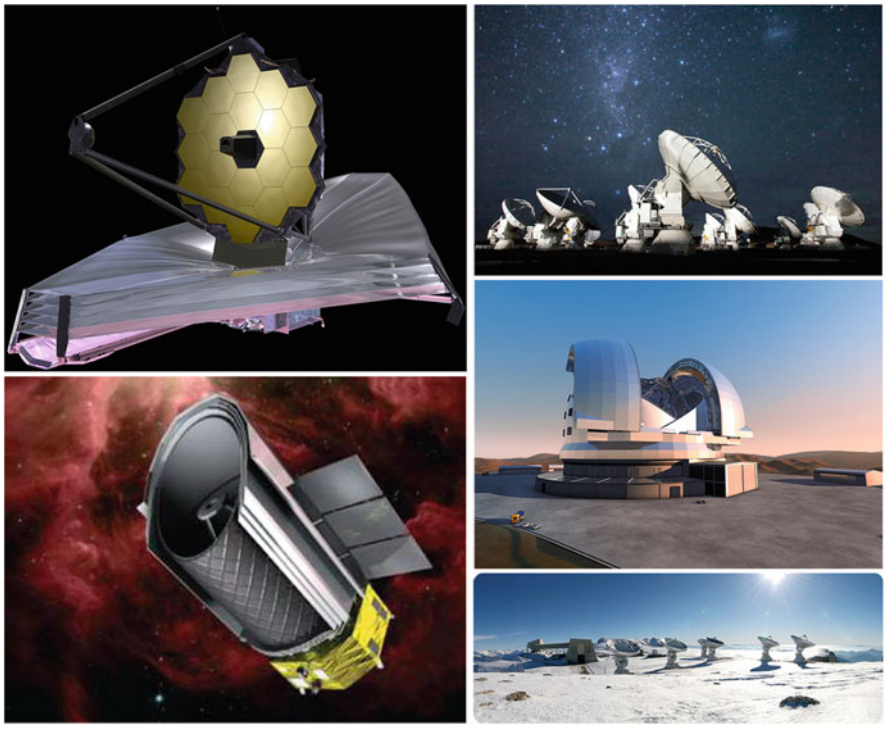

Fig. 2.8 Sketches of planned or proposed future telescopes. From left to right, *top row*: the space telescopes JWST (James Webb Space Telescope, currently in construction, image credit NASA) and SPICA (JAXA project, image credit JAXA); *bottom row*: the ground based telescopes ALMA (in construction, image credit ESO/NOAJ/NRAO), Extremely Large Telescope (ELT, ESO project), Plateau de Bure Interferometer (PdBI) (in operation, proposal for extension as NOEMA, image credit IRAM)

With the increase in the size and sensitivity of visible and near infrared cameras, it is now possible to map the extinction across large areas of the sky, covering the full extent of molecular complexes [51]. These studies make use of full sky surveys such as the Two Micron Sky Survey (2MASS [52]) and the associated stellar catalogue to derive extinction maps. To reach very large column densities, access to the infrared wavelength region has proven to be the most valuable tool. First images of the Galactic Plane at 8 μm revealed dark patches, reminiscent of the classical dark clouds, that were therefore named "infrared dark clouds". As explained above, some of these infra red dark clouds are now thought to be the birth place of massive stars. Current catalogues include 10,000 of objects [20].

The efficiency of scattering as a function of wavelength of the incoming radiation is a strong function of the particle size. Therefore a large fraction of current information on the particle size distribution has been extracted from analysis of the scattered light, in visible nebulae as well as at infrared wavelengths to probe the

population of dust grains in dense cores. While the classical population of dust grains has sub-micron size (0.1 μm) in the diffuse clouds and in visible nebulae, the analysis of the deep images taken by the IRAC camera on board the Spitzer satellite has revealed the presence of significantly bigger grains, with micrometre sizes [53] likely resulting from the coagulation and aggregation of smaller particles.

2.5.1.2 Far Infrared

In the far infrared, the continuum radiation from the interstellar medium is dominated by the dust thermal emission. At long wavelengths in the far infrared and sub-millimetre domains, the emission is dominated by the sub-micrometre dust grains that reach a stable temperature. The resulting emission can be described by a modified black-body law, namely:

$$I(\nu) = \varepsilon(\nu)(2k_B\nu^2)/c^2 1/(e^{h\nu/k_BT} - 1) \tag{2.5}$$

where ε(ν) describes the emissivity of dust grains as a function of frequency, and T is the dust grain temperature. ε can be derived either empirically from the analysis of multi-wavelength observations, or from theoretical models of the dust grain composition and structure. To first order, ε scales as ν^{β}, with β ranging between 1.5 and 2. The assumption of a single dust grain temperature is a simplification given the spread in dust grain size and composition, but is usual in order to obtain a first insight into the mean properties of the source. The mean grain temperature is about 18 K [54, 55] in the diffuse interstellar medium, and decreases to ∼12 K in dense clouds and even down to ∼6 K in the coldest dense pre-stellar cores [26] (Fig. 2.7).

The spectra of interstellar nebulae deviate notably from a modified black-body at short and mid-infrared wavelengths (from about 3 to 60 μm), with a significantly stronger radiation than that expected from thermal produced by the smallest solid particles of nanometre size, that can fluctuate in temperature following the absorption of a far UV photon. This phenomenon can heat the small particles to temperatures of a few hundred Kelvin, sufficient to emit in the mid infrared [3].

Therefore, by combining information across the electromagnetic spectrum, it is possible to reveal the dust content, temperature and spatial distribution, as well as the direction of the heating sources.

2.5.1.3 Polarimetry

The analysis of light polarization properties is the best tool to probe the magnetic field in the interstellar medium. Indeed, there are two main mechanisms producing polarized radiation in the visible and near infrared: (1) through scattering of the incoming radiation from a nearby star, or (2), as a result of the dust grain partial alignment with the magnetic field. These two mechanisms can be easily identified

with their different spatial and spectral properties. In the former case, the polarization is detected at the same wavelength as the incoming radiation and has a specific spatial pattern determined by the source geometry. In the latter case, the polarization of radiation is caused by asymmetries in the light absorption by dust grains, induced by the magnetic fields. Sub-micron dust grains are not perfectly spherical and can therefore induce an alignment of the long axis of the dust grains perpendicular to the local direction of the magnetic field. Such a geometry is indeed a stable configuration since spinning elongated particles tend to align their angular momentum with the local direction of the magnetic field. The most likely grain alignment mechanism is thought to be due to radiative torques (e.g. [56] and references therein) induced by asymmetry in the grain illumination and their irregular shapes. Aligned grains absorb with higher efficiency light polarized with the electric field parallel to the long axis of the dust grain. Therefore aligned dust grains create a polarization pattern in the extinction of background stars, with the direction of polarization parallel to the direction of the magnetic field. While the dust alignment is a local effect, the resulting polarization pattern is a global effect since the signal is integrated along the line of sight. The efficiency of polarization amounts to a few percent, but its dependency on the intensity of the field is not completely understood yet. The most useful information is the direction of polarization, which gives the direction of the component of the magnetic field parallel to the plane of the sky. Aligned dust grains also cause a polarization pattern in their thermal radiation at far infrared and sub-millimetre wavelength, because the efficiency of thermal radiation is larger in the direction parallel to their long axis. The resulting polarization pattern is perpendicular to the extinction polarization pattern, with the polarization angle being perpendicular to the local direction of the magnetic field.

In both cases, the direction of polarization gives access to the average direction of the magnetic field, projected on the plane of the sky. No information is available on the magnetic field component along the line of sight with this method. The polarization degree ranges from a few percent up to slightly more than 10%.

A third method for studying the magnetic field is the detection of the Zeeman effect using molecular lines. The presence of a magnetic field breaks the degeneracy of the energy levels of molecule. This effect induces a splitting of the molecular spectral lines, together with specific polarization pattern in the different spectral components. The current detection schemes make use of these properties. Usually, the Zeeman effect is detected in circular polarization, resulting from the difference between the left hand side and the right hand side polarizations. The magnitude of this effect scales with the intensity of the magnetic field along the line of sight. The number of suitable spectral lines for such studies is relatively limited, because it requires paramagnetic molecules that strongly interact with the magnetic field. Such species have spectral lines which can be significantly split in the presence of the magnetic field. In the interstellar medium, the hyperfine structure line of atomic hydrogen at 21 cm, the Λ doubling lines of OH at 18 cm, and the rotational lines of the CN radical near 113 GHz are the main spectral features used for measuring the magnetic field [42].

2.5.2 Spectroscopy

Spectroscopy is a key method of investigation for astrochemistry. It can be combined with imaging methods in so-called "spectro-imaging techniques", which provide three dimensional data cubes, having as first two dimensions the position on the sky, and as third dimension a spectral axis, labelled in wavelength, frequency or velocity.

Spectroscopy is a very important technique because it allows measurements of most of the constituents of the interstellar gas, thanks to their unique spectral signatures (see Chap. 1) (Fig. 2.9). Depending on the wavelength domain, molecules, atoms and ions in the gas phase can be detected through their electronic, vibrational, rotational and/or fine-structure transitions. Given the typical values of the Doppler broadening of interstellar lines of a few km s^{-1}, high spectral resolution is required for obtaining spectral information on the line profiles, namely $R = \lambda/\delta\lambda \geq 10^4$. This figure is a minimum, with higher spectral resolutions reaching 10^6 being favoured for studies requiring a detailed description of the line profiles. Given the low pressures of the interstellar medium, the sole broadening mechanism of spectral lines is the Doppler effect. It relates the shift in line frequency ν (or wavelength λ) relative to the rest frequency $\nu_0(\lambda_0)$ to the velocity of the molecule or atom v_z along the line of sight joining the source and the telescope. To first order, it can be written as,

$$\delta v/v_0 = (v - v_0)/v_0 = -\delta\lambda/\lambda_0 = -v_z/c \tag{2.6}$$

Therefore line profiles carry precious information on the gas dynamics along the line of sight, as the Doppler effect is only sensitive to the velocity component parallel to the direction of observation. The centroid of the line profile provides the mean velocity along the line of sight, the line width provides information on the velocity dispersion that can have several sources:

- Thermal broadening resulting from the random motions of molecules or atoms at a finite temperature, $\sigma_{th} = \sqrt{k_B T/m}$
- Turbulent motions associated with the local fluid dynamics, σ_t.
- Systematic motions along the line of sight, such as ordered rotation, expansion or more complex motions.

The first two broadening mechanism produce Gaussian line profiles,

$$f(v) = (1/\sigma\sqrt{\pi})e^{-(v-v0)^2/\sigma^2} \tag{2.7}$$

with v_0 the source velocity in the rest frame of interest, and σ the broadening parameter, while the last mechanism can produce any line profile, either symmetric or asymmetric. It is therefore customary to use Gaussian profiles to fit astronomical line profiles. For this purpose, astronomers often use the Full Width at Half

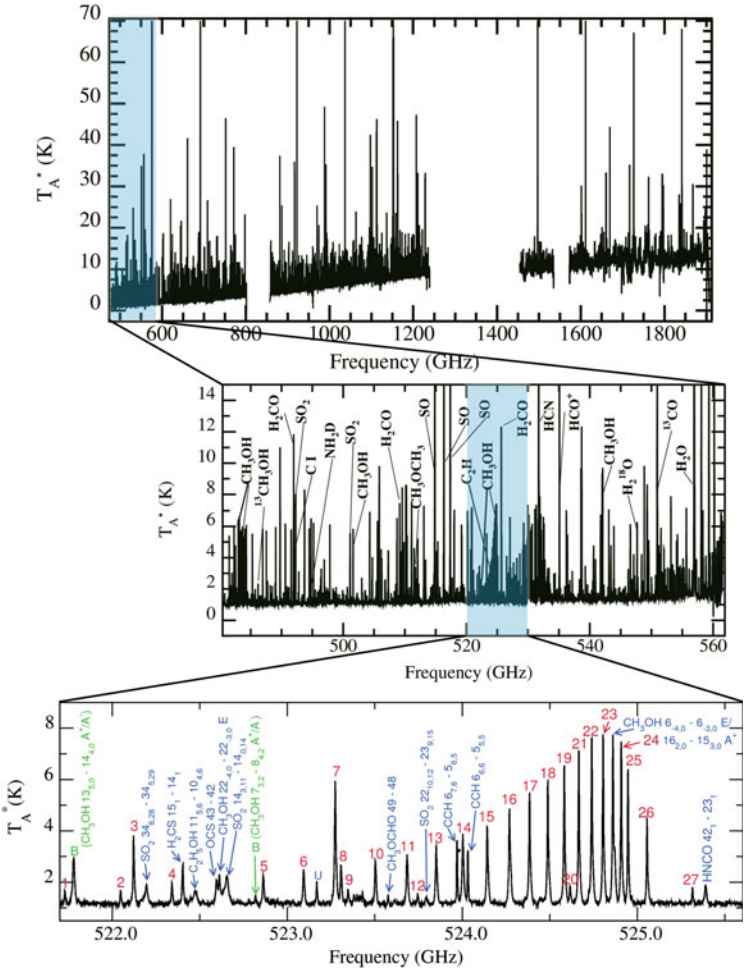

Fig. 2.9 (continued)

Maximum *FWHM* to characterize the line width. It is related to the broadening parameter σ with $FWHM = 2\sigma\sqrt{ln(2)} \sim 1.665\sigma$.

Although their spectral signatures are not as narrow as gas phase species, the composition of the dust particles can also be established through analysis of astronomical spectra, especially in the infrared spectral domain. The best tools are the vibrational bands of solid state materials. For instance, two deep absorption bands at 9.7 and 18 μm track the presence of silicate grains. The exact position and shape of the band carry important information on the silicate composition, amorphous versus crystalline character, as well as the grain sizes. The physical meaning is as follows: these bands correspond to the elongation and bending modes of the Si − O bond in silicates whose properties depend on the environment of these

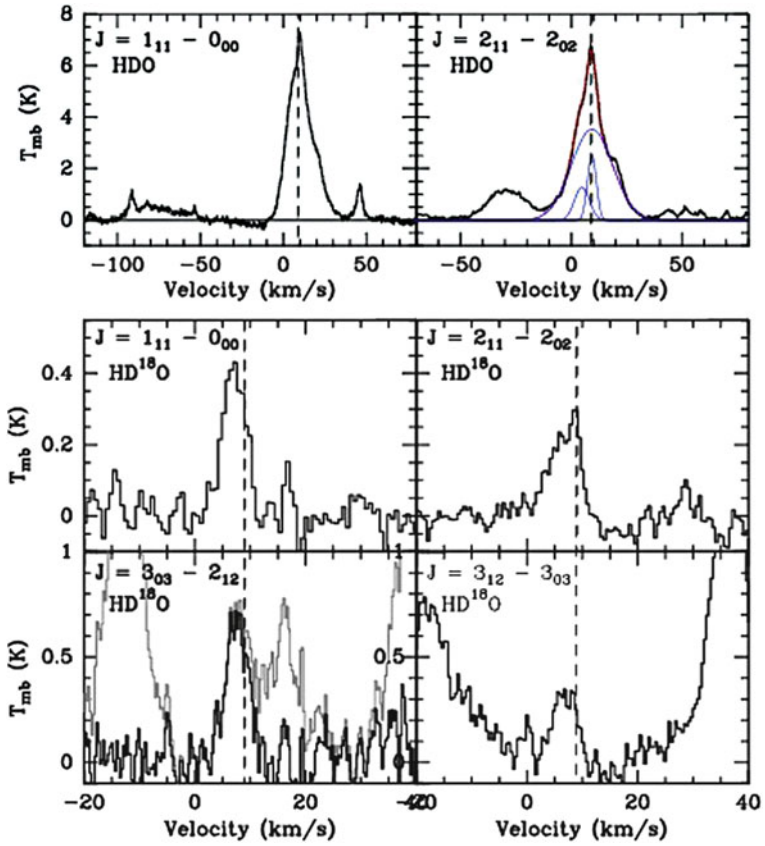

Fig. 2.9 Subset of the full spectral survey of the Orion-KL region performed with the Herschel space observatory. The *first panel* shows the frequency coverage with two successive zooms on a small subset of the data, where the carriers of the strongest lines are identified. In the *bottom panel*, all lines with numbers ranging from 1 to 27 are produced by CH_3OH. The *second panel* shows a collection of lines from HDO and $HD^{18}O$. The line profile is fitted with four separate spectral components, corresponding to four spatially distinct sources of emission, that are too close to be spatially separated at the moderate angular resolution allowed by Herschel [57]

atoms in the solid. The dependency with the grain size is introduced because a competition between absorption and scattering will be dimming the bands when grains reach a size comparable to the wavelength of the band [3].

The presence of mantles on silicate grains is revealed by absorption bands of water ice, superimposed with features from carbon monoxide, carbon dioxide, methanol and other less abundant constituents. As for the silicate bands, the spectral features associated with molecular ices are most prominent in the infrared spectral region, between 3 and 40 μm mainly. Because water ice is the main constituent of ice mantles, the spectral features due to water ice are the strongest, especially the 3.1 μm feature due to the stretching mode of the O-H bound in solid water. This band can be fully saturated for deeply embedded young stellar objects.

2.5.3 Instruments

Specific instruments have been developed to enable the detection of the faint and usually extended emission of interstellar nebulae, as well as the narrow spectral lines, that can appear either as emission or absorption features. The key parameters for such studies are the spatial and spectral resolution of the instruments, their wavelength coverage and sensitivity. Depending on the wavelength domain, specific detectors and instrument layout must be used that take advantage of the most recent advances in light collecting and detection.

For a telescope of diameter D, the scattering of the incoming radiation upon the dish provides the most stringent limit on the angular resolving power $\delta\theta$ defined as the angular size of the smallest object that can be individually resolved. This resolving power is related to the telescope diameter and the observing wavelength λ as

$$\delta\theta \sim \lambda/D \sim 1''(\lambda/1\mu m)(0.25m/D)$$

In this formula, the resolving power is expressed in arcsec ($1rd = 206265''$). The theoretical resolution is seldom achieved at visible wavelengths because the atmospheric turbulence limits the resolving capabilities of ground based telescopes to a fraction of an arcsec, unless they are equipped with adaptive optics correcting systems. In the far infrared and (sub)millimetre domain, the seeing induced by the atmosphere has no impact and telescopes can achieve their theoretical angular resolution. For the closest molecular clouds situated in the Taurus or Ophiuchus complexes, at distances d of about 120 parsecs, such a resolving power corresponds to a linear size l of $l = \delta\theta d = 1.8 \times 10^{13}$ m ~ 120 AU ~ 0.6×10^{-3} pc.

In the following, we give a short summary of the main observatories and instruments that have led to great advances in the field of astrochemistry.

Instruments operating at ultraviolet wavelengths must be space borne as the Earth's atmosphere efficiently shields the energetic radiation. Recent instruments include the Hubble Space Telescope (HST) with its long suite of instruments combining imaging cameras and spectrometers (see http://hubblesite.org/the_telescope/). The Far Ultraviolet Spectrum Explorer (FUSE) has explored the shortest wavelength, a key domain for the study of molecular hydrogen.

In the visible, ground based telescopes provide the necessary instruments, with imaging cameras with a large field of view and sensitive high resolution spectrometers. Similar instruments are developed in the near infrared spectral region, that is well accessible from the ground. (see e.g. the instrument available at the European Southern Observatory (ESO) http://www.eso.org).

The atmospheric transmission becomes very poor past ~10 μm, with the increased attenuation of the mid and far infrared radiation by molecules in the atmospheres, most notably water vapour H_2O and carbon dioxide CO_2. Therefore the information has been acquired using space borne or airborne telescopes such as the ESA mission Infrared Space Observatory (ISO http://sci.esa.int/iso) and

the NASA Spitzer Space Telescope (http://www.spitzer.caltech.edu), or the Stratospheric Observatory for Infrared Astronomy (SOFIA), (http://www.sofia.usra.edu). The need for space borne systems is also true in the far infrared. This wavelength domain is currently accessible thanks to SOFIA and the joint ESA/NASA mission Herschel Space Observatory (http://herschel.esac.esa.int).

The sky becomes more transparent at longer wavelengths, allowing the use of large (sub)millimetre telescopes from ground based observatories. Because the presence of water vapour in the atmosphere is one of the major source of atmospheric opacity, these observatories are located in high altitude sites such as the top of the Mauna Kea extinct volcano or the high altitude Chajnantor plateau in the Atacama desert about 5,000 m above sea level in Chile. This frequency domain, from about 80 GHz to about 900 GHz is one of the main sources of information for studying interstellar molecules since it corresponds to the frequencies of rotational lines of molecules. However, the relatively long wavelength gives access to limited spatial resolution as the spatial resolution power of a given telescope scales linearly with the wavelength and inversely with its size, as λ/D. Therefore at (sub) millimetre wavelengths, even the largest monolithic telescopes like the IRAM 30 m telescope (http://www.iram-institute.org) have a modest spatial resolution of several tens of arcsec, significantly worse than the arcsec achievable with visible and IR telescopes because of the long wavelengths. Therefore, it is customary to build radio interferometers, in which the incoming radiation is coherently detected by several identical dishes spaced by a large distance, from a few hundred meters up to several kilometres. The resolving power is now given by the telescope separation, rather than by the telescope diameter, enabling an excellent spatial resolution. The price to pay is in terms of sensitivity, especially for extended emission since the sparse spacing of the telescopes composing the interferometer (typically six to nine element telescopes, giving access to $N(N-1)/2$ independent measurement points) introduces a spatial filtering in the incoming radiation.

The Plateau de Bure Interferometer (PdBI) located in the French Alps, and the Atacama Large (sub)Millimeter Array (ALMA) (http://www.almaobservatory.org/) located in Chile are among the most sensitive (sub)millimetre radio interferometers. When its construction is complete, ALMA will provide unprecedented sensitivity for detection and imaging, with its 50 antenna network and its complementary arrays increasing the sensitivity to extended emission.

References

1. Bertoldi F, Cox P, Neri R et al (2003) High-excitation CO in a quasar host galaxy at $z = 6.42$. Astron Astrophys 409:47
2. Noterdaeme P, Petitjean P, Srianand R, Ledoux C, López S (2011) The evolution of the cosmic microwave background temperature. Measurements of T_{CMB} at high redshift from carbon monoxide excitation. Astron Astrophys 526:L7
3. Draine B (2011) Physics of the interstellar and intergalactic medium, Princeton series in astrophysics. Princeton University Press, Princeton

4. Ostriker EC, McKee CF, Leroy AK (2010) Regulation of star formation rates in multiphase galactic disks: a thermal/dynamical equilibrium model. Astrophys J 721:975
5. Wood KH, Alex S, Joung MR, Mac Low MM, Benjamin RA, Haffner LM, Reynolds RJ, Madsen GJ (2010) Photoionization of high-altitude gas in a Supernova-driven turbulent interstellar medium. Astrophys J 721:1397
6. Field GB, Goldsmith DW, Habing HJ (1969) Cosmic-ray heating of the interstellar gas. Astrophys J 155:L149
7. Jenkins EB, Tripp TM (2011) The distribution of thermal pressures in the diffuse, cold neutral medium of our galaxy. II. An expanded survey of interstellar C I fine-structure excitations. Astrophys J 734:65
8. Heiles C, Troland TH (2005) The millennium Arecibo 21 centimeter absorption-line survey. IV. Statistics of magnetic field, column density, and turbulence. Astrophys J 624:773
9. Audit E, Hennebelle P (2010) On the structure of the turbulent interstellar clouds. Influence of the equation of state on the dynamics of 3D compressible flows. Astron Astrophys 511:A76
10. Rachford BL, Snow TP, Destree JD et al (2009) Molecular hydrogen in the far ultraviolet spectroscopic explorer translucent lines of sight: the full sample. Astrophys J Suppl 180:125
11. Miville-Deschênes M-A, Martin PG, Abergel A et al (2010) Herschel-SPIRE observations of the Polaris flare: structure of the diffuse interstellar medium at the sub-parsec scale. Astron Astrophys 518:L10
12. Roman-Duval J, Jackson JM, Heyer M, Rathborne J, Simon R (2010) Physical properties and galactic distribution of molecular clouds identified in the galactic ring survey. Astrophys J 723:492
13. Kolmogorov A (1941) The local structure of turbulence in incompressible viscous fluid for very large Reynolds' numbers. DoSSR 30:301
14. Falgarone E, Hily-Blant P, Pety J (2009) Intermittency of interstellar turbulence: extreme velocity-shears and CO emission on milliparsec scale. Astron Astrophys 507:355; Lis DC, Vaillancourt JE, Goldsmith PF, Bell TA, Scoville NZ, Zmuidzinas J (eds) (2009) Submillimeter astrophysics and technology: a symposium honoring Thomas G. Phillips. ASP conference series, vol 417. Astronomical Society of the Pacific, San Francisco, p 243
15. Lada CJ, Lombardi M, Alves J (2010) On the star formation rates in molecular clouds. Astrophys J 724:687
16. André P et al (2010) From filamentary clouds to prestellar cores to the stellar IMF: initial highlights from the Herschel Gould Belt Survey. Astron Astrophys 518:L102
17. Alves JF, Lada CJ, Lada EA (2001) Internal structure of a cold dark molecular cloud inferred from the extinction of background starlight. Nature 409:159
18. Caselli P, van der Tak FFS, Ceccarelli C, Bacmann A (2003) Abundant H_2D^+ in the pre-stellar core L1544. Astron Astrophys 403:L37
19. Pérault M, Omont A, Simon G (1996) First ISOCAM images of the Milky Way. Astron Astrophys 315:L165
20. Peretto N, Fuller GA (2010) A statistical study of the mass and density structure of infrared dark clouds. Astrophys J 723:555
21. Herbst E, van Dishoeck E (2009) Complex organic interstellar molecules. Annu Rev Astron Astrophys 47:427
22. Parise B, Castets A, Herbst E, Caux E, Ceccarelli C, Mukhopadhyay I, Tielens AGGM (2004) First detection of triply-deuterated methanol. Astron Astrophys 416:159
23. Stark R, Sandell G, Beck SC et al (2004) Probing the early stages of low-mass star formation in LDN 1689 N: dust and water in IRAS 16293-2422A, B, and E. Astrophys J 608:341
24. Commerçon B, Hennebelle P, Audit E, Chabrier G, Teyssier R (2010) Protostellar collapse: radiative and magnetic feedbacks on small-scale fragmentation. Astron Astrophys 510:L3
25. Mouschovias T, Spitzer L (1976) Note on the collapse of magnetic interstellar clouds. Astrophys J 210:326
26. Bergin E, Tafalla M (2007) Cold dark clouds: the initial conditions for star formation. Annu Rev Astron Astrophys 45:339

27. Pety J, Gueth F, Guilloteau S, Dutrey A (2006) Plateau de Bure interferometer observations of the disk and outflow of HH 30. Astron Astrophys 458:841
28. Burrows CJ, Stapelfeldt KR, Watson AM (1996) Hubble space telescope observations of the disk and jet of HH 30. Astrophys J 473:437
29. Levinson HF, Morbidelli A, Tsiganis K, Nesvorný D, Gomes R (2011) Late orbital instabilities in the outer planets induced by interaction with a self-gravitating planetesimal disk. Astron J 142:152
30. Lagrange AM, Bonnefoy M, Chauvin G et al (2010) A giant planet imaged in the disk of the young star β Pictoris. Science 329:57
31. Gerin M, Pety J, Goicoechea JR (2009) The horsehead nebula, a template source for interstellar physics and chemistry. In: Lis DC, Vaillancourt JE, Goldsmith PF, Bell TA, Scoville NZ, Zmuidzinas J (eds) Submillimeter astrophysics and technology: a symposium honoring Thomas G. Phillips. ASP conference series, vol 417. Astronomical Society of the Pacific, San Francisco, p 165
32. Gonzalez GM, Le Bourlot J, le Petit F, Roueff E (2008) Radiative transfer revisited for emission lines in photon dominated regions. Astron Astrophys 485:127
33. Glover SCO, Federrath C, Mac Low MM, Klessen RS (2010) Modelling CO formation in the turbulent interstellar medium. Mon Notices R Astron Soc 404:2
34. Draine BT, Mc Kee CF (1993) Theory of interstellar shocks. Annu Rev Astron Astrophys 31:373
35. Nisini B, Benedettini M, Codella C et al (2010) Water cooling of shocks in protostellar outflows: *Herschel*-PACS map of L1157. Astron Astrophys 518:L120
36. Troscompt N, Faure A, Wiesenfeld L, Ceccarelli C, Valiron P (2009) Rotational excitation of formaldehyde by hydrogen molecules: ortho-H_2CO at low temperature. Astron Astrophys 493:687
37. Maret S, Faure A, Scifoni E, Wiesenfeld L (2009) On the robustness of the ammonia thermometer. Mon Notices R Astron Soc 399:425
38. van der Tak FFS, Black JH, Schöier FL, Jansen DJ, van Dishoeck EF (2007) A computer program for fast non-LTE analysis of interstellar line spectra with diagnostic plots to interpret observed line intensity ratios. Astron Astrophys 468:627
39. Goicoechea JR, Pety J, Gerin M, Hily-Blant P, Le Bourlot J (2009) The ionization fraction gradient across the Horsehead edge: an archetype for molecular clouds. Astron Astrophys 498:771
40. Indriolo N, McCall BJ (2012) Investigating the cosmic-ray ionization rate in the galactic diffuse interstellar medium through observations of H_3^+. Astrophys J 745:91
41. Neufeld D, Goicoechea JR, Sonnentrucker P et al (2010) Herschel/HIFI observations of interstellar OH^+ and H_2O^+ towards W49N: a probe of diffuse clouds with a small molecular fraction. Astron Astrophys 521:L10
42. Crutcher RM (2009) OH and CN Zeeman observations of magnetic fields in molecular clouds. Rev Mex de Astron y Astrofisica (Serie de Conferencias) 36:107
43. Godard B, Falgarone E, Pineau Des Forets G (2009) Models of turbulent dissipation regions in the diffuse interstellar medium. Astron Astrophys 495:847
44. Gibb EL, Whittet DCB, Boogert ACA, Tielens AGGM (2004) Interstellar ice: the infrared space observatory legacy. Astrophys J 151:35
45. Motte F, Zavagno A, Bontemps S et al (2010) Initial highlights of the HOBYS key program, the Herschel imaging survey of OB young stellar objects. Astron Astrophys 518:L77
46. Joblin C, Tielens AGGM (eds) (2011) PAHs and the universe: a symposium to celebrate the 25th anniversary of the PAH hypothesis. EAS publications series, vol 46. EDP Sciences, Les Ulis
47. Jura M (1974) Formation and destruction rates of interstellar H_2. Astrophys J 191:375
48. Le Bourlot J, Le Petit F, Pinto C, Roueff E, Roy F (2012) Surface chemistry in the interstellar medium – I – H2 formation by Langmuir-Hinshelwood and Eley-Rideal mechanisms. Astron Astrophys 541:A76

49. Danger G, Bossa J-B, de Marcellus P, Borget F, Duvernay F, Theulé P, Chiavassa T, D'Hendecourt L (2011) Experimental investigation of nitrile formation from VUV photochemistry of interstellar ices analogs: acetonitrile and amino acetonitrile. Astron Astrophys 525:30
50. de Marcellus P, Bertrand M, Nuevo M, Westall F, Le Sergeant d'Hendecourt L (2011) Prebiotic significance of extraterrestrial ice photochemistry: detection of hydantoin in organic residues. Astrobiology 11:847
51. Lombardi M, Alves J, Lada CJ (2011) 2MASS wide field extinction maps. IV. The Orion, Monoceros R2, Rosette, and Canis Major star forming regions. Astron Astrophys 535:A16
52. Skrutskie MF, Cutri RM, Stiening R et al (2006) The two micron all sky survey (2MASS). Astron J 131:1163
53. Pagani L, Steinacker J, Bacmann A, Stutz A, Henning T (2010) The ubiquity of micrometer-sized dust grains in the dense interstellar medium. Science 329:1622
54. Planck Collaboration, Abergel A, Ade PAR, Aghanim N et al (2011) *Planck* early results. XXIV. Dust in the diffuse interstellar medium and the galactic halo. Astron Astrophys 536:24
55. Compiègne M, Verstraete L, Jones A, Bernard J-P, Boulanger F, Flagey N, Le Bourlot J, Paradis D, Ysard N (2011) The global dust SED: tracing the nature and evolution of dust with DustEM. Astron Astrophys 525:A103
56. Whittet DCB, Hough JH, Lazarian A, Hoang T (2008) The efficiency of grain alignment in dense interstellar clouds: a reassessment of constraints from near-infrared polarization. Astrophys J 764:304
57. Bergin E, Phillips TG, Comito C et al (2010) Herschel observations of EXtra-Ordinary Sources (HEXOS): the present and future of spectral surveys with Herschel/HIFI. Astron Astrophys 521:L20

http://www.springer.com/978-3-642-31729-3

Astrochemistry and Astrobiology
Smith, I.W.M.; Cockell, C.S.; Leach, S. (Eds.)
2013, X, 350 p., Hardcover
ISBN: 978-3-642-31729-3